Available online at www.sciencedirect.com
SCIENCE DIRECT
Geochimica et Cosmochimica Acta 70 (2006) 3139–3148
Geochimica
www.elsevier.com/locate/gca

Kinetic isotope effect during reduction of iron from a silicate melt

B.A. Cohen [a,*], S. Levasseur [b], B. Zanda [a,c], R.H. Hewins [a,c], A.N. Halliday [d]

[a] Department of Geological Sciences, Rutgers University, Piscataway, NJ, USA
[b] Department of Earth Sciences, ETH Zentrum, NO, Sonneggstrasse 5, Zürich CH8092, Switzerland
[c] Laboratoire d'Etude de la Matière Extraterrestre, Muséum National d'Histoire Naturelle, Paris, France
[d] Department of Earth Sciences, University of Oxford, Parks Road, Oxford OX1 3PR, United Kingdom

Received 22 September 2005; accepted in revised form 29 March 2006

Abstract

Iron isotopic compositions measured in chondrules from various chondrites vary between $\delta^{57}Fe/^{54}Fe = +0.9‰$ and $-2.0‰$, a larger range than for igneous rocks. Whether these compositions were inherited from chondrule precursors, resulted from the chondrule-forming process itself or were produced by later parent body alteration is as yet unclear. Since iron metal is a common phase in some chondrules, it is important to explore a possible link between the metal formation process and the observed iron isotope mass fractionation. In this experimental study we have heated a fayalite-rich composition under reducing conditions for heating times ranging from 2 min to 6 h. We performed chemical and iron isotope analyses of the product phases, iron metal and silicate glass. We demonstrated a lack of evaporation of Fe from the silicate melt in similar isothermal experiments performed under non-reducing conditions. Therefore, the measured isotopic mass fractionation in the glass, ranging between $-0.32‰$ and $+3.0‰$, is attributed to the reduction process. It is explained by the faster transport of lighter iron isotopes to the surface where reduction occurs, and is analogous to kinetic isotope fractionation observed in diffusion couples [Richter, F.M., Davis, A.M., Depaolo, D.J., Watson, E.B., 2003. Isotope fractionation by chemical diffusion between molten basalt and rhyolite. *Geochim. Cosmochim. Acta* **67**, 3905–3923]. The metal phase contains 90–99.8% of the Fe in the system and lacks significant isotopic mass fractionation, with values remaining similar to that of the starting material throughout. The maximum iron isotope mass fractionation in the glass was achieved within 1 h and was followed by an isotopic exchange and re-equilibration with the metal phase (incomplete at ~6 h). This study demonstrates that reduction of silicates at high temperatures can trigger iron isotopic fractionation comparable in its bulk range to that observed in chondrules. Furthermore, if metal in Type I chondrules was formed by reduction of Fe silicate, our observed isotopic fractionations constrain chondrule formation times to approximately 60 min, consistent with previous work.
© 2006 Elsevier Inc. All rights reserved.

1. Introduction

Chondrules are crystalline millimeter-size igneous spherules found in primitive chondritic meteorites. They contain olivine, pyroxene, metal, sulfide, and glass of varying compositions. The relationship between their bulk compositions and textures provides evidence that chondrule precursors were heated close to their liquidus temperatures, 1400–1750 °C (Radomsky and Hewins, 1990), possibly by shock waves (Desch and Connolly, 2002) in the solar nebula (Taylor et al., 1983). Chondrules are generally divided into FeO-rich (Type II) and FeO-poor (Type I) (McSween, 1977), with the latter containing significant amounts (up to 10 vol.%) of Fe–Ni metal (Reisener and Goldstein, 1999). The metal, in addition to iron and nickel, also contains sulfur, cobalt, chromium, and phosphorus.

The amount of metal varies between different chondrite types, and metal-silicate fractionation is of sufficient importance that metal abundance has been used in classifying chondrites (Larimer and Wasson, 1988; Sears and Dodd, 1988). In the CR meteorites, among the chondrites with the highest metal content, metal grains are principally found within chondrules and around chondrule rims, suggesting formation or modification of metal during

* Corresponding author.
E-mail address: bosmat.cohen@gmail.com (B.A. Cohen).

0016-7037/$ - see front matter © 2006 Elsevier Inc. All rights reserved.
doi:10.1016/j.gca.2006.03.022

chondrule formation. In other chondrites, e.g. OC, much metal occurs between chondrules, with size-density relations suggesting aerodynamic sorting, which may explain metal-silicate fractionation (Cuzzi et al., 2001; Zanda et al., 2002).

The metal grains that are zoned with respect to Ni, as found in some chondrite groups (CH and CB) (Weisberg and Prinz, 1999) are agreed to have originated as direct condensates, either from the solar nebula (Meibom et al., 1999; Campbell and Humayun, 2004) or from an impact plume (Krot et al., 2005). They are also strongly zoned in Fe and Ni isotopes, with light cores, suggesting rapid condensation (Alexander and Hewins, 2004). By contrast, the origin of metal in other types of chondrites is still debated. Grossman and Wasson (1985) suggested that metal formed as condensate and remained unmodified by the chondrule-forming process, apart from segregating from the silicate. Zanda et al. (1994), Hewins et al. (1997), and Cohen and Hewins (2004) argued for a metal origin as residue from the evaporation of S from sulfide melt in chondrules. Others suggested that chondrule metal has originated during the chondrule-forming process through reduction of FeO-bearing silicates either by the reduced protosolar nebula or by reduced carbon in the chondrule precursors (Connolly et al., 1994; Connolly et al., 2001). A third group proposed metal evaporation during chondrule formation followed by recondensation during cooling (Kong and Palme, 1999; Zanda et al., 2002).

Because of the importance of metal in understanding the details of chondrule formation and nebular fractionations, the isotopic composition of Fe in chondrules has been investigated. Alexander and Wang (2001) used an ion microprobe to measure $\delta^{57/56}$Fe (compared to the composition observed in the San Carlos Olivine) in olivines from Chainpur (LL3.4) chondrules, including highly magnesian ones that might have formed by evaporation of FeO from a chondritic precursor. Their measurements do not exhibit a significant isotopic mass fractionation in $\delta^{57/56}$Fe (values fell within their measurement uncertainty of ~1–2‰), and the absence of the Rayleigh fractionation associated with free evaporation led to the proposition that back-reaction of chondrules with the ambient gas suppressed isotopic fractionation. Recently, a more precise measurement technique (i.e. MC-ICPMS) was used to demonstrate that isotopic mass fractionation of iron in chondrules, though small, is significant. Mullane et al. (2003a,b) performed analyses on the silicate portion of chondrules from Allende (CV > 3.6) (Bonal et al., in press) and Chainpur, and found $\delta^{57/54}Fe_{IRMM\text{-}014}$ values ranging between +0.6‰ and −1.9‰, where

$$\delta^{57}\mathrm{Fe} = [(^{57}\mathrm{Fe}/^{54}\mathrm{Fe})_{\mathrm{sample}}/(^{57}\mathrm{Fe}/^{54}\mathrm{Fe})_{\mathrm{IRMM\text{-}14}} - 1] \times 1000(‰). \quad (1)$$

The standard used for calculating $\delta^{57/54}$Fe was IRMM-014 (Standard from the Institute for Reference Materials and Measurements, European Commission). Kehm et al. (2003) measured iron isotope composition compositions in chondrules from Tieschitz (H3.6) and reported $\delta^{56/54}Fe_{Kil1919}$ values ranging between −0.5‰ and 0.0‰. They interpreted the range in Fe-isotope composition of chondrules as the result of Fe loss during condensation, assuming that gas and condensate do not maintain equilibrium. Mullane et al. (2003a,b) suggested that the origin of the isotopic variability displayed by chondrules lies in mass-dependent isotopic heterogeneities inherited from their precursors. Mullane et al. (2005) showed that Fe isotopes in Type I chondrules are heavier than in Type IIs, which is consistent with more evaporation in the type Is. If reduction causes isotopic fractionation, it would also be consistent with more reduction in the type I chondrules. Mullane et al. (2005) also found modifications of the primary isotopic compositions of chondrules, especially for small chondrules.

Isotopic analyses of metal in chondrules have not been made so far, but isolated metal in chondrites has been analyzed (Gildea et al., 2005) and it appears to be heavier than bulk chondrules. Metal in five pallasites has higher δ^{57}Fe than coexisting olivine, and iron meteorites are slightly heavier than bulk chondrites (Poitrasson et al., 2005). The discovery (Poitrasson et al., 2005) of a heavier Fe isotopic composition in taenite in iron meteorites than in kamacite which grew from it demonstrates the potential role of diffusion in processes other than evaporation for developing isotopic fractionations.

None of the previous studies have explored the possibility of a link between the presence of iron metal in chondrules and the range of Fe-isotope fractionation displayed by the silicate portion of chondrules. Kinetic isotope effects are known in association with redox processes (Niles et al., 2005). In this study we have conducted heating experiments in which we have reduced an FeO-rich silicate melt. The metal produced and the residual silicate glasses were analyzed for chemical and iron isotope compositions. Our objective here was to study the effects, if any, of the reduction process on the isotopic make up of the ensuing metal and silicate phases and to determine whether our results may offer new insights into iron isotope fractionation in chondrules.

2. Experiments

To obtain very FeO-rich silicate melt, we chose as starting material a synthetic sample containing large hopper fayalite crystals, a slag. The bulk composition was determined on a glass prepared at an oxygen fugacity equivalent to half a log unit above the iron-wustite buffer or IW+0.5 and for 10 min at 1480 °C. The mean of 19 analyses made on a JEOL 8600 electron probe is listed in Table 1. Under the formation conditions, there was no evaporative loss of Na, or Fe in 60 min (Table 1), and there was no reduction.

Experiments were conducted in a 1-atm vertical Deltech furnace. Isothermal experiments were conducted at 1450, 1500, and 1540 °C. For each temperature run, between 80

Table 1
Chemical compositions and their corresponding standard deviations of powdered starting material melted at 1480 °C and IW+0.5 for 10 (chosen to best represent the starting material), 30, and 60 min. Its isotopic composition was measured on unheated powdered starting material

Oxide wt%	10 min	SD	30 min	SD	60 min	SD
SiO_2	33.59	0.76	33.78	0.84	33.44	0.68
Al_2O_3	6.83	0.19	6.88	0.20	6.79	0.17
TiO_2	0.26	0.02	0.24	0.03	0.25	0.02
FeO	47.25	0.58	47.76	0.55	47.20	0.45
MnO	5.47	0.12	5.54	0.13	5.52	0.12
MgO	1.60	0.12	1.75	0.13	1.83	0.13
CaO	2.59	0.09	2.55	0.08	2.52	0.08
K_2O	0.43	0.05	0.38	0.04	0.36	0.04
Na_2O	0.28	0.06	0.30	0.07	0.32	0.05
Total	98.30	0.77	99.18	0.99	98.22	0.89
δ^{57}Fe	−0.32‰	2s = 0.03‰				

and 81 mg of starting material set in a graphite crucible was placed in the hot spot of a furnace containing either pure CO, or a CO/CO_2 mix with an oxygen fugacity equivalent to or IW−0.5. Heating times varied between 2 min and 6 h (Table 2). The charges were quenched by placing the bottom of the crucible in water. Some of the metal occurred as very fine beads attached to the walls of the crucible and, based on the pattern of weights recovered versus run time, up to half the metal produced was lost. Based on the mass of FeO, SiO, and MnO remaining in the silicate bead, up to 12.5 mg of oxygen was lost in each run.

Duplicate runs were made. One of the silicate beads from each pair of experiments was analyzed on a JEOL 8600 electron probe for chemical composition, using an accelerating potential of 20 kV and a current of 15–20 nA. Counting times varied between 20 and 40 s. Glass analyses were performed using a 5 μm rastered beam. Some analyses were performed on a Cameca SX100 microprobe at Université Paris VI. Silicate beads were analyzed using a 5 μm defocused beam, a current of 10 nA and an acceleration of 15 kV. Metal beads were analyzed using a focused beam, a 40 nA current and an acceleration of 15 kV.

Iron isotope compositions were determined on material from the duplicate charges using a Nu Plasma MC-ICPMS

Table 2
Chemical analyses of the experimental charges. Concentrations displayed in weight percent. Also shown is Fe isotopic compositions of the silicate and metal phase in each charge. Isotopic composition and 2s are shown in ‰

Time (min)	wt%									Total	δ^{57}Fe metal (‰)	2s	δ^{57}Fe silicate (‰)	2s
	SiO_2	Al_2O_3	TiO_2	FeO	MnO	MgO	CaO	K_2O	Na_2O					
1450 °C														
2											−0.31	0.25		
5	45.7	9.3	0.33	31.3	7.3	2.3	3.4	1.0	0.31	101.04			0.13	0.07
10	53.7	11.9	0.45	13.7	10.4	3.1	4.3	1.8	0.49	99.84	−0.34	0.25		
20	58.0	13.1	0.48	6.9	11.1	3.8	4.8	2.0	0.51	100.85	−0.29	0.08	−0.12	0.04
30	59.8	13.5	0.49	4.2	11.2	3.2	4.9	2.1	0.43	99.75	−0.42	0.10	0.63	0.09
40	63.0	12.7	0.47	4.6	9.4	2.9	4.7	2.0	0.44	100.14	−0.33	0.03	1.03	0.11
60	59.7	13.6	0.52	2.0	11.4	3.7	5.2	2.2	0.46	98.69	−0.23	0.10	2.25	0.07
90	62.2	14.3	0.54	0.66	10.9	3.9	5.3	2.2	0.45	100.51	−0.26	0.09	2.62	0.06
120	64.4	13.7	0.52	0.51	9.4	3.6	5.2	2.1	0.46	99.88				
240	64.8	14.4	0.51	0.29	7.6	3.6	5.5	2.2	0.38	99.26	−0.20	0.03	2.02	
360	65.4	15.2	0.51	0.17	6.5	3.7	5.8	2.0	0.21	99.42	−0.01	0.16	1.71	
1500 °C														
5	53.9	10.9	0.40	18.2	8.5	2.7	4.0	1.5	0.42	100.55	−0.38	0.12		
10	56.1	12.8	0.52	5.2	11.4	3.6	5.1	2.1	0.49	97.18	−0.38	0.14	−0.24	0.20
20	57.9	13.2	0.53	3.6	11.4	3.6	5.2	2.1	0.46	98.11	−0.36	0.13	0.77	
30	60.3	13.4	0.54	1.5	11.6	3.7	5.3	2.1	0.46	98.90	−0.26	0.10	2.03	0.18
60	59.9	14.2	0.56	0.30	10.0	4.0	5.7	2.1	0.42	97.27	−0.30	0.05	2.32	0.32
90											−0.12	0.08	2.33	0.11
120	60.6	15.4	0.55	0.18	8.8	4.3	6.1	2.0	0.32	98.23	−0.22	0.08		
240	63.7	16.3	0.53	0.21	6.1	3.9	6.3	1.9	0.19	99.00	−0.28	0.05	1.90	
360	53.9	10.9	0.40	18.2	8.5	2.7	4.0	1.5	0.42	100.55	−0.22	0.06	0.05	
1540 °C														
5	57.3	11.6	0.43	11.8	9.2	3.0	4.4	1.7	0.43	99.78	−0.46	0.17	−0.17	0.08
10	57.9	13.2	0.54	3.5	11.3	3.6	5.2	2.1	0.50	97.96	−0.16	0.17	0.32	0.07
20	59.1	13.8	0.54	0.78	11.4	3.9	5.6	2.1	0.47	97.68	−0.21	0.15	2.60	0.08
30	59.3	14.2	0.58	0.53	10.8	4.0	5.7	2.2	0.48	97.79	−0.30	0.13	2.77	0.10
60	59.7	15.7	0.57	0.16	9.1	4.3	6.3	2.1	0.35	98.17	−0.47	0.03	2.93	0.03
90											−0.31	0.06	2.76	0.30
120	63.3	16.2	0.51	0.21	6.6	4.1	6.2	2.1	0.38	99.68				
240											−0.13	0.18	1.05	
360	60.9	20.0	0.50	0.17	3.5	4.7	7.8	1.5	0.05	99.21	−0.25	0.02	0.42	

(multiple collector inductively coupled plasma mass spectrometer) at ETH-Zürich using a standard bracketing technique (Levasseur et al., 2004). The iron isotopic compositions, shown in Table 2, are expressed in δ^{57}Fe, relative to the IRMM-014 standard. All the Fe isotopic data lie on a mass-dependent fractionation line with a slope of one-third when plotted as $\delta^{57/54}$Fe against $\delta^{57/56}$Fe (Fig. 1), indicating that hydrides and other putative interferences are insignificant. It should be noted that the normalization to IRMM-14 used here is shifted from the one based on the igneous Fe base line (also called Earth–Moon igneous average) adopted by some authors (Beard and Johnson, 1999). The δ^{57}Fe value of IRMM-14 relative to the igneous Fe base line $= -0.11‰ \pm 0.14‰$ (2σ) (Johnson et al., 2003). This means that

$$\delta^{57}Fe_{IRMM\text{-}14} = \delta^{57}Fe_{IGNEOUS} + 0.11. \quad (2)$$

The normalization to Kil1919, as practiced by Kehm et al. (2003) should correspond very closely to the Earth–Moon igneous average. All the iron isotope data discussed below will be expressed in $\delta^{57/54}Fe_{IRMM\text{-}14}$ using the notation δ^{57}Fe.

The isotopic composition of the starting material was determined on the original powdered slag. Analyses of run products were made on five separate fractions: metal beads detached from the silicate, fine metal beads separated from the silicate using 3 N HCl overnight, silicate glass without obvious fine metal, reduced to powder, powder which is leached with 3 N HCl, and the leachate which is the complement of the latter. This was to check that metal was uniform in composition, and that no remaining iron metal affects the composition of the silicate. About 10 mg of powdered glass were used for the analyses. The amount of metal was a function of the size of the beads available but was at least a few mg. The leachates were separated from the glass powder by centrifugation for 15 min at 10^4 rpm. The powder was then rinsed twice with MilliQ-Element water, this water being eliminated also by centrifugation.

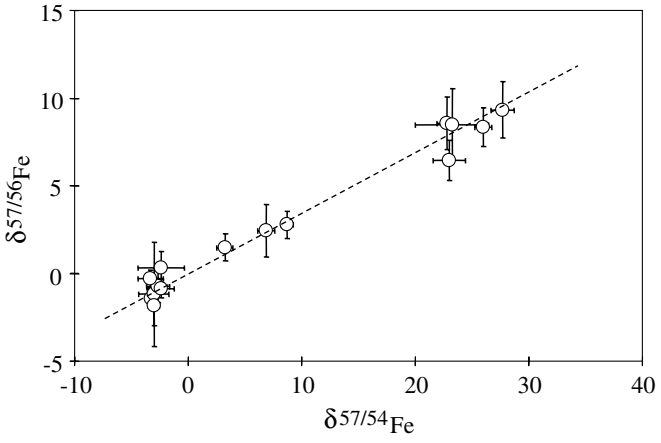

Fig. 1. Iron isotopic data plotted on a $\delta^{57/54}$Fe against $\delta^{57/56}$Fe diagram. Data points lie on a mass-dependent fractionation line with a slope of one-third indicating that hydrides and other putative interferences are insignificant.

The metal beads were dissolved in a mixture of 0.5 ml distilled 6 N HCl and 0.5 ml of 16 N HNO_3 and the powders of silicate glass were dissolved in a mixture of 0.5 ml distilled HNO_3 and 0.5 ml of distilled 27 N HF. Once dissolved, samples (and leachates) were evaporated and re-dissolved in 6 N HCl and evaporated again. Before its passage on an anion exchange column, the sample was finally re-dissolved in 1 ml of 6 N HCl. More information on this procedure can be found in Levasseur et al. (2004).

The results show that metal and silicate are uniform and that the leaching step has no significant effect, i.e. the powdered glass, the leached glass, and the leachate all had the same isotopic composition. The long-term reproducibility of the standard (internal laboratory standard made of dissolved hematite) is $\delta^{57}Fe = 0.87‰ \pm 0.12‰$ (2σ) over the duration of the study.

3. Results

Experimental charges were studied by electron microprobe and BSE imaging, and all consist of only two major phases, a silicate glass and metal beads (containing sulfide blebs). The charges for the shortest heating times (2–5 min) consist of glass and tiny metal beads embedded in the glass (Cohen et al., 2005). Due to relatively short heating durations these charges contain many vesicles. In the charges heated for longer durations (greater than 10 min) the metal beads become larger and are confined to the circumference of the silicate bead (Fig. 2). In these experiments a large separate metal bead was produced as well. At even longer heating times the metal and silicate separate completely. In these experiments the glass bead is entirely free of any metal (Fig. 2).

The chemical analyses of the glass beads are shown in Table 2. They are homogeneous, with standard deviations 1–3% of the amount present for major elements. Cr and Ni are below the detection limits of the electron probe. The most noticeable and obvious change in the glass compositions is the decrease in the concentration of FeO, which decreases steeply in the first hour of heating, from 47 to 13.6 wt% at 1450 °C and 3.5 wt% at 1550 °C after 10 min, and then tapers off (Table 2, FeO normalized to Al_2O_3 shown in Fig. 3). The rate of decrease increases with run temperature. In runs we made under similar conditions, except for an fO_2 above the iron-wustite buffer, there is no Fe loss (Fig. 3). Experiments on a less FeO-rich composition (Yu et al., 2003) show a barely significant evaporative loss of Fe at 1.0×10^{-5} bar at 1450 °C for the same heating time.

In Fig. 4 we examine the behavior of Na as a function of heating time. In the time it takes for more than 90% of the FeO to be lost, there are very modest evaporative losses of Na, whereas in vacuum about 95% of the Na would be lost

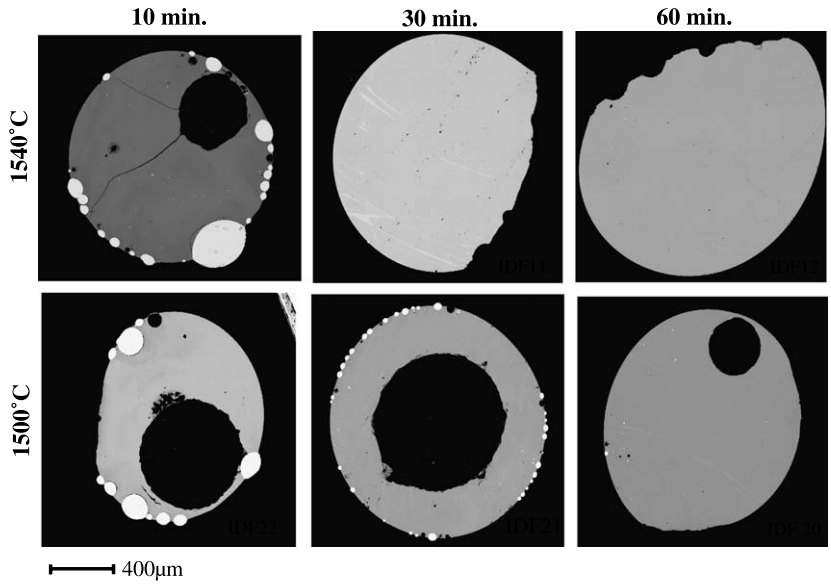

Fig. 2. BSE images of experimental charges heated at 1500 and 1540 °C for 10, 30, and 60 min. Metal formed during short runs (10–30 min) is found both as small beads around the rim of the charge and in a separated bead (not shown). During longer experiments (60 min and longer) all the metal that formed coalesced into one separate bead (not shown) leaving the glass clear of metal.

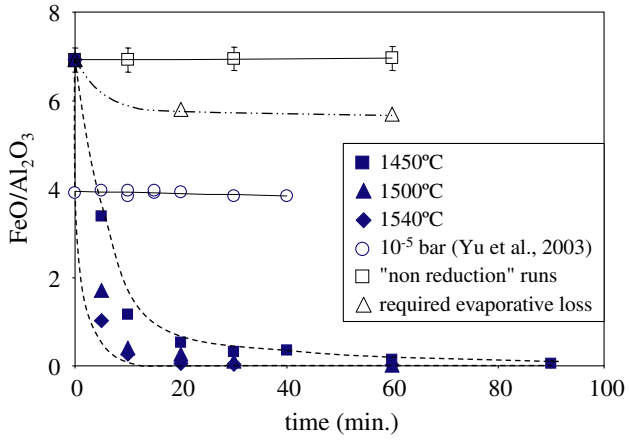

Fig. 3. FeO/Al_2O_3 ratios vs. time (min) in the charges produced in the 1450, 1500, and 1540 °C reduction runs (solid symbols), together with data from our "non-reduction" runs (open squares) conducted at 1480 °C, 1 atm and IW+0.5. Open triangles represent calculated values of the minimum amount of iron loss expected from Rayleigh evaporation, based on the $\delta^{57}Fe$ values of the 20 and 60 min runs at 1540 °C (solid line through these points was hand drawn). Also shown are data from experiments by Yu et al. (2003) conducted at 1450 °C and 1.0×10^{-5} bar (open circles). Dashed lines represent upper and lower limits for the results of the reduction experiments.

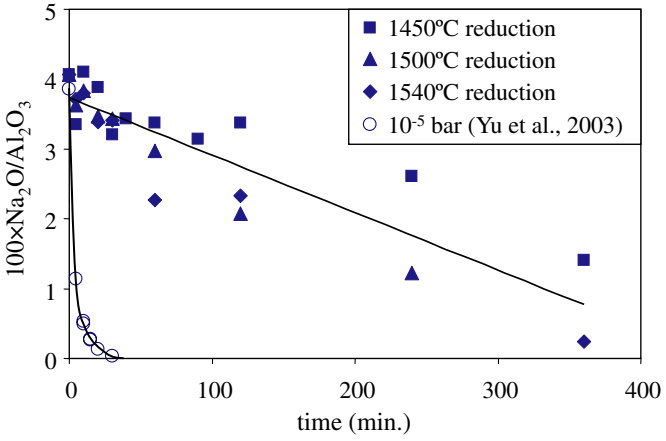

Fig. 4. $100 \times Na_2O/Al_2O_3$ vs. time (min) in the charges produced at the 1450, 1500, and 1540 °C experimental runs (solid symbols), together with data from experiments by Yu et al. (2003) conducted at 1450 °C and 1.0×10^{-5} bar (open circles).

(Yu et al., 2003). There are similar small evaporative losses of K in our experiments (Table 2). Manganese, a less volatile element, decreases with time too (Table 2), but is incorporated into the metal–sulfide liquid.

The metal beads (Table 3) are comprised overwhelmingly of iron (over 91 wt%) together with other elements such as Si (up to 0.8 wt%), S (up to 4.0 wt%), Cu (1.0 wt%), Mn (0.71 wt%), and P (0.22 wt%). While the concentrations of Mn and P in the metal remained constant in the different experimental runs, those of S and Cu gradually decreased with longer heating time. Manganese is incorporated into the metallic component and is observed as the sulfide alabandite (Fig. 5), containing 43 wt% Mn, 20 wt% Fe, and 2 wt% Cu (Table 3). Some troilite is also present.

The results of the iron isotope analyses of the metal and silicate glass beads are shown in Table 2 and in Fig. 6. The initial iron isotope composition of the starting material was measured as −0.32‰ using unheated powdered starting material. In runs for all three temperatures, the iron isotope composition of the glass increases rapidly within the first 60–80 min to +2.5–3‰. As experimental run times become longer the isotopic

Table 3
Chemical composition of metal grains in a number of experimental charges

	No. of points	Si	P	S	Mn	Fe	Co	Cu	Total
1500 °C									
10 min	5	0.02	0.14	2.58	0.12	94.78	0.09	0.74	98.50
	SD	0.02	0.04	1.44	0.07	1.09	0.03	0.12	0.33
20 min	4	0.40	0.11	1.80	1.05	93.91	0.10	0.68	98.10
	SD	0.07	0.05	1.19	1.94	3.25	0.02	0.14	0.04
30 min	4	0.69	0.11	0.39	0.14	95.53	0.07	0.46	97.42
	SD	0.10	0.02	0.16	0.10	0.14	0.03	0.04	0.17
1540 °C									
10 min	5	0.11	0.12	1.26	0.13	95.85	0.08	0.62	98.20
	SD	0.03	0.04	0.92	0.10	1.03	0.02	0.09	0.13
30 min	1	2.11	0.08	0.57	1.57	91.94	0.03	0.32	96.62
Alabandite		0.02	0.02	34.33	42.58	20.52	0.02	2.14	99.63

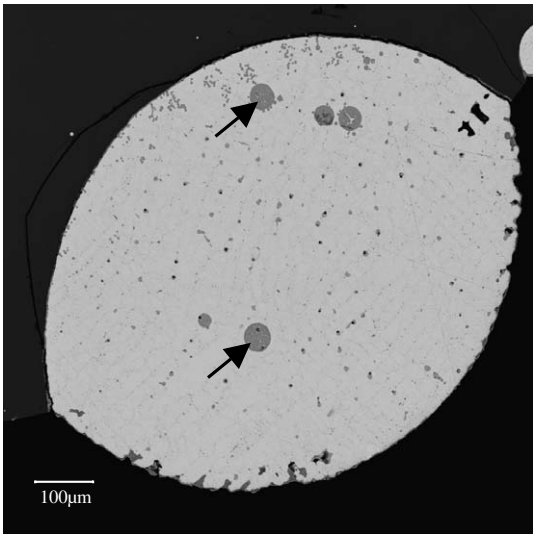

Fig. 5. BSE image of a metal grain on the rim of a silicate bead produced at a 10 min run at 1540 °C. The arrows point to two alabandite grains containing 43 wt% Mn, 20 wt% Fe, and 2 wt% Cu.

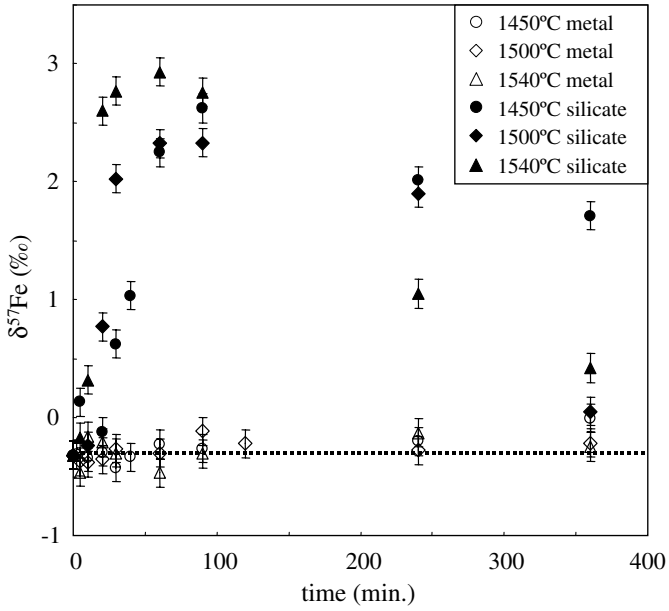

Fig. 6. δ^{57}Fe (‰) for the silicate phase (solid symbols) and for the metal phase (open symbols) formed in the experimental runs of 1450, 1500, and 1540 °C. Error bars are based on the long-term reproducibility of the standard. The heavy dashed line represents the initial δ^{57}Fe value of the starting material, i.e. −0.32‰.

composition of the silicate gradually decreases, approaching the value of its starting material. The isotopic composition of the iron metal (containing 90–99.8% of the Fe in the system) shows almost no fractionation and the values hover around the starting material value of −0.32‰.

The bulk δ^{57}Fe composition of the different charges is shown in Table 4 and in Fig. 7 Bulk isotopic composition for each charge was calculated following:

$$f\mathrm{Fe}_{\mathrm{silicate}} \times \delta^{57}\mathrm{Fe}_{\mathrm{silicate}} + f\mathrm{Fe}_{\mathrm{metal}} \times \delta^{57}\mathrm{Fe}_{\mathrm{metal}}, \quad (3)$$

where $f\mathrm{Fe}_{\mathrm{silicate}}$ and $f\mathrm{Fe}_{\mathrm{metal}}$ stand for the fraction of Fe in the silicate and metal phase, respectively. Iron fractions were calculated using final weights (Table 4) and FeO wt% from electron probe analyses (Table 2). For the purpose of this calculation we assumed that the metal is composed solely of Fe. The bulk isotopic compositions of the charges fall between 0‰ and −0.5‰, which is close to the starting material value of −0.32‰.

4. Discussion

4.1. Evaporation versus reduction

The lack of iron metal in the starting material coupled with the abundant metal found in the final charges shows that the steep drop in FeO in the silicates is without question dominantly the product of FeO reduction. However, reduction is not the only process that could cause FeO to diminish. Since evaporation might have played a role, it is essential to evaluate what portion, if any, of the observed decrease in FeO could be attributed to evaporative loss. Understanding the relative role of each of these processes is essential for the ultimate interpretation of the isotopic data.

Table 4
Final weights of the silicate and metal, the total Fe in both phases and the bulk Fe isotopic composition

Time	Metal weight (mg)	Silicate weight (mg)	Total Fe (mg)	Bulk δ^{57}Fe (‰)
1450 °C				
20	12.20	50.30	14.92	−0.26
30	19.30	43.80	20.72	−0.35
40	16.40	46.10	18.01	−0.21
60	19.20	46.70	19.94	−0.14
90	11.50	49.30	11.76	−0.20
1500 °C				
5	15.80	52.1	23.45	−0.25
10	11.10	53.5	13.24	−0.36
20	23.70	42.8	24.88	−0.30
30	23.30	41.5	23.77	−0.22
60	20.40	39.7	20.49	−0.29
90	47.90	14.60	47.93	−0.11
240	37.00	22.40	37.04	−0.27
360	57.00	1.60	57.00	−0.22
1540 °C				
5	14.80	47.00	19.36	−0.39
10	16.40	43.00	17.59	−0.13
20	20.30	42.20	20.56	−0.18
30	19.40	39.30	19.56	−0.28
60	22.00	36.00	22.05	−0.46
360	11.60	43.70	11.60	−0.25

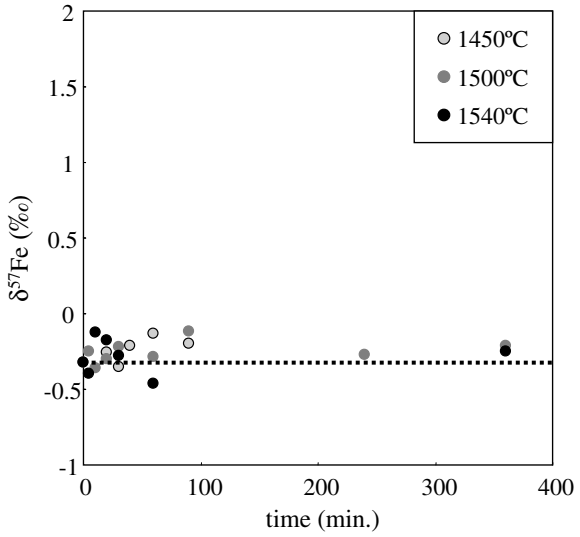

Fig. 7. Calculated bulk-δ^{57}Fe composition of the charges produced during the 1450, 1500, and 1540 °C runs, based on the δ^{57}Fe values and weights of the silicate and metal phases (Table 4). The heavy dashed line represents the initial δ^{57}Fe value of the starting material, i.e. −0.32‰.

FeO loss by evaporation at 1 bar is not normally detectable, though Fe may be lost from a charge to a Pt support wire or gained from an Fe-coated Pt wire. Mass balance could not be used in this case to estimate evaporative losses, because up to 12.5 mg of oxygen was lost per run, and some of the reduced Fe occurred as minute spherules attached to the crucible walls. Mass recovered as a function of heating time is erratic, with up to 8 mg of the expected Fe lost. We also performed some isothermal experiments at 1480 °C under non-reducing conditions (IW+0.5). As shown in Fig. 3, these runs show constant FeO. Even in vacuum heating experiments (Yu et al., 2003) there are only very slight evaporative losses of FeO at 1450 °C (Fig. 3). At 1580 °C at 1.3×10^{-5} bar, up to 50% of the initial FeO is still present after 4 h (Cohen et al., 2004).

The volatility of FeO is significantly lower than that of Na_2O (Cohen et al., 2004). In low pressure experiments, Na is totally depleted from the silicate melt within an hour, while FeO losses are barely significant statistically (Figs. 2 and 3; Yu et al., 2003). In the present work, Na shows very modest losses in the first hour (Fig. 4), whereas FeO is constant in the same time under oxidizing conditions (Fig. 3).

Additional convincing evidence for the absence of evaporation of FeO lies in the near uniform value of the bulk-δ^{57}Fe composition of the experimental charges (Fig. 7) and in this value being so close to that of the starting composition. This is because in the charges for which isotopic measurements were made, between 90% and 99.8% of the mass of Fe in the run products, is present in the metallic phase: any change to the isotopic composition of the metal would be <0.3‰ and could not be resolved. Evaporation of Fe from metallic melt is much faster than evaporation of FeO from silicate melt (Cohen and Hewins, 2004; Cohen et al., 2004). Evaporation of our charges would preferentially remove ^{54}Fe from the metallic portion of the charge leaving it with a heavier isotopic composition than the silicate. The opposite is observed.

We can interpret the Fe data for our reduction experiments in the context of Rayleigh evaporation. During Rayleigh distillation the isotopic composition of the residual fraction (the silicate melt) follows:

$$\delta - \delta_o \cong 10^3(\alpha - 1) \cdot \ln f, \quad (4)$$

where δ_o is the initial isotope composition, δ is the isotopic composition after the process occurs, f is the remaining fraction, and α is the equilibrium fractionation factor for the reaction and is equal to $\sqrt{(m_1/m_2)} = 0.9733$. The maximum isotopic fractionation of 2.9‰ corresponds to retention of 0.8865 of the original fraction of FeO. The retained FeO normalized to Al is shown in Fig. 3, and we do not observe such a loss in our runs made under non-reducing conditions. If the hypothetical evaporation was non-Rayleigh, the required losses of FeO would be even greater.

Complementary experiments to ours have been performed by Roskosz et al. (2005). They heated a haplobasaltic melt in contact with Pt for 24 h at 1500 °C, at different oxygen fugacities. The silicate is depleted, and the Pt enriched, in Fe as a function of decreasing oxygen fugacity, though the reaction is two orders of magnitude slower than reduction with C. Roskosz et al. (2005) found that the $\delta^{56/54}$Fe composition of the silicate became heavier with increased reduction of FeO, with a total enrichment varying between 0.1‰ and 4.8‰ for 30 min, and 24 h, respectively. This is larger than what is observed in this study, and confirms that reduction of Fe metal from silicate causes a

kinetic isotope effect. They were also able to demonstrate that the initial Fe metal had a significantly lighter isotopic composition, because their reduction rate was so much slower that Pt with low concentrations of Fe could be recovered.

4.2. Reduction and isotopic diffusion

The iron isotope mass fractionation measured in the experimental charges occupies a range of about 3‰, remarkably similar to the one measured in chondrules (Mullane et al., 2003a,b) and possibly related to the processes that occurred in the natural objects. In the previous section we eliminated iron evaporation as the process behind the measured isotopic fractionation, leaving only reduction of FeO into Fe-metal. The coexistence of metal and silicate alone would not explain the isotopically heavy nature of the silicates, as at equilibrium the silicate is lighter (Beard and Johnson, 1999; Zhu et al., 2002; Poitrasson et al., 2005). We assume that the rate of diffusion of the iron isotopes through the silicate melt to its surface is purely mass dependent, with lighter isotopes possessing the higher diffusion rates. In this way the mass fractionation measured in our shorter experiments resulted from the light ^{54}Fe arriving at the surface to be transferred to metal faster than ^{57}Fe, with this effect reaching a maximum after 60 min. This diffusion-controlled fractionation found during reduction was confirmed in experiments by Roskosz et al. (2005). It is analogous to kinetic isotope fractionation observed in diffusion couples (Richter et al., 2003) and to the development of a heavier Fe isotopic composition in taenite in iron meteorites than in kamacite which grew from it (Poitrasson et al., 2005).

As the iron reservoir in the silicate phase nears depletion, with the remaining iron enriched in the heavy isotope, the reduction process becomes extremely sluggish. From this point, forward isotopic exchange of Fe between the metal and the silicate phase becomes the dominant process. Both reduction and exchange must occur to some extent throughout each experiment, but the difference between the rates of reduction and isotopic exchange does not remain the same. As the process of reduction approaches completion and the amount of metal produced nears 100%, the process of isotopic exchange becomes dominant. Isotopic exchange gives an approach to isotopic equilibrium between the two phases, i.e. higher δ^{57}Fe in metal than coexisting olivine as in pallasites (Poitrasson et al., 2005), though it is not reached after 6 h. While this process was in effect since the start of the experiments, it is only when the reduction process is virtually complete that isotopic exchange plays a noticeable role. The long tail in the isotopic composition of the silicate phase, seen in Fig. 6, is the result of this process.

The results of this study bear a remarkable resemblance to those of Skulan et al. (2002, Fig. 9). In their experimental study Skulan et al. (2002) investigated Fe isotopic fractionation between aqueous Fe(III) and hematite at 98 °C. Their results showed that over short time scales kinetic isotopic fractionation dominates, whereas over longer time scales isotopic fractionation between the two phases nears zero due to re-equilibration. Despite the striking differences in the conditions of the two experiments the fundamental dynamic processes affecting isotopic compositions are the same.

4.3. The effect of temperature

Our experimental results show that there is a temperature effect on the extent of iron isotope fractionation in the silicate phase and perhaps on the rate at which the fractionation occurs. Experiments conducted at 1540 °C produced mass fractionations that were ~0.5‰ higher than charges produced at lower temperatures. The charges produced at 1500 °C are slightly heavier than those of 1450 °C for short run times, but subsequently do not occupy an intermediate position between the 1540 and 1450 °C runs. The peak of isotopic fractionation appears to have been reached at about 60 min in the 1540 °C runs, which is earlier than the peak achieved at lower temperatures (~90 min). The effect of temperature on the extent of isotopic mass fractionation may be due to the increase in diffusion rates with increasing temperature.

4.4. Implications for chondrules

Chondrules show some of the largest Fe-isotope fractionations measured in igneous materials. Allende chondrules are both heavier and lighter than chondrite matrix, which has an Fe isotopic composition close to that of the Earth (Mullane et al., 2005). Although these experiments were not intended to simulate chondrule formation environments, they share key features with those environments. The temperatures of these experiments, ranging between 1450 and 1540 °C, the reducing environment and the iron-bearing starting composition are similar to formation conditions and precursors suggested for chondrules. Most importantly we have created an iron metal, in a similar way to that suggested for metal in chondrules (Connolly et al., 2001), and showed that this process can result in an isotopic mass fractionation comparable to that measured in chondrules.

Therefore, if metal in chondrules was formed through reduction of iron-bearing silicate precursors in the presence of carbon and/or hydrogen, we can use the extent of mass fractionation to estimate their formation times. Gauging from our experimental results, a mass fractionation of ~2.5‰ exhibited by chondrules, translates to a heating duration of about 60 min for a Type I metal-rich chondrule heated once. Such heating times are in accordance with proposed heating mechanisms for chondrules (Desch and Connolly, 2002).

Four Type I and three Type II Allende chondrules were characterized and analyzed for Fe isotopes by Mullane et al. (2005). The Type I chondrules have the heaviest Fe

isotopes, with $\delta^{56/54}Fe_{IRMM\text{-}014} \sim 0‰$ to $+0.7‰$, the Type IIs the lightest, $\sim 0‰$ to $-1.4‰$. This pattern would rule out one possibility, parent body alteration suggested by Kehm et al. (2003). It is consistent with diffusion-controlled loss of FeO from the Type I chondrules, with the amount of fractionation being more consistent with reduction than evaporation. Fe isotopic variations in highly oxidized Type II chondrules imply a complex history. Some are very light (Mullane et al., 2003a,b, 2005) and might be explained by partial condensation (Kehm et al., 2003), possibly recondensation of light Fe evaporated from Type I chondrules either by adding it to the dust precursor or by directly adding it to chondrule melts. Chondrules with minor or accessory opaques show only modest fractionations (Mullane et al., 2005), suggesting complementary isotopic compositions for metal and silicates. Isolated metal in equilibrated chondrites has been analyzed (Gildea et al., 2005) and it appears to be heavier than bulk chondrules, reflecting equilibration. Iron isotope analyses of the iron metal phase in chondrules are crucially necessary for further understanding the thermal history of chondrules and the origin of their metals.

5. Conclusions

In this study, we have closely monitored the evolving isotopic composition of an Fe-bearing silicate as it underwent reduction at high temperatures. The same material heated under oxidizing conditions showed no evaporative loss of FeO. At the beginning of the reduction process the glass underwent an initial ^{57}Fe-enrichment, with a peak enrichment of $\sim 3‰$ at 1 h, attributed to the different diffusion rates of iron isotopes within the silicate melt. As the reduction neared completion, isotopic exchange (which became the dominant process) caused a gradual decrease in the isotopic composition of the glass, which dragged it close to that of the metal and the initial value.

In previous studies the measured $2.5‰$ range in $^{57}Fe/^{54}Fe$ displayed by chondrules was interpreted to result from initial precursor heterogeneities, evaporation and recondensation or parent body alteration processes. Here we propose yet another interpretation in which we link the observed mass fractionation to the reduction of silicate material while forming metal in Type I chondrules. Furthermore, provided the metal in chondrules was indeed formed by the reduction of iron-bearing silicate precursors, the results of this study suggests heating times of about 60 min.

Acknowledgments

We thank Greg Herzog and François Robert for discussions, and Kevin Righter and an anonymous reviewer for comments which led to considerable improvements in the manuscript.

Associate editor: Christian Koeberl

References

Alexander, C.M.O'D., Hewins, R.H., 2004. Mass fractionation of Fe and Ni isotopes in metal in Hammadah al Hamrah 237 Meteorit. *Planet Sci.* **39**, A13, abstract.

Alexander, C.M.O'D., Wang, J., 2001. Iron isotopes in chondrules: Implications for the role of evaporation during chondrule formation. *Meteorit. Planet. Sci.* **36**, 419–428.

Beard, B.L., Johnson, C.M., 1999. High precision iron isotope measurements of terrestrial and lunar material. *Geochim. Cosmochim. Acta* **63**, 1653–1660.

Bonal, L., Quirico, E., Bourot-Denise, M., Montagna, G., 2006. Determination of the petrologic type of CV3 chondrites by Raman spectroscopy of included organic matter. *Geochim. Cosmochim. Acta* **70**, 1849–1863.

Campbell, A.J., Humayun, M., 2004. Formation of metal in the CH chondrites ALH 85085 and PCA 91467. *Geochim. Cosmochim. Acta* **68**, 3409–3422.

Cohen, B.A., Hewins, R.H., 2004. An experimental study of the formation of metallic iron in chondrules. *Geochim. Cosmochim. Acta* **68**, 1677–1689.

Cohen, B.A., Hewins, R.H., Alexander, C.M.O'D., 2004. The formation of chondrules by open-system melting of nebular condensates. *Geochim. Cosmochim. Acta* **68**, 1661–1675.

Cohen, B.A., Levasseur, S., Zanda, B., Hewins, R.H. Halliday, A.N. 2005. Isotopic mass fractionation of iron in chondrules, evaporation or reduction? In: *Lunar Planet. Sci. XXXVI.* Lunar Planet. Inst., Houston. CD-ROM #7654 (abstract).

Connolly Jr., H.C., Hewins, R.H., Ash, R.D., Zanda, B., Lofgren, G.E., Bourot-Denise, M., 1994. Carbon and the formation of reduced chondrules. *Nature* **371**, 136–139.

Connolly Jr., H.C., Huss, G.R., Wasserburg, G.J., 2001. On the formation of Fe–Ni metal in Renazzo-like carbonaceous chondrites. *Geochim. Cosmochim. Acta* **65**, 4567–4588.

Cuzzi, J.N., Hogan, R.C., Paque, J.M., Dobrovolskis, A.R., 2001. Size-selective concentration of chondrules and other small particles in protoplanetary nebula turbulence. *Astrophys. J.* **546**, 496–508.

Desch, S.J., Connolly Jr., H.C., 2002. A model of the thermal processing of particles in solar nebula shocks: application to the cooling rates of chondrules. *Meteorit. Planet. Sci.* **37**, 183–207.

Gildea, K.J., Burgess, R., Lyon, I.C., Sears, D.W., 2005. Iron isotope geochemistry of metal grains in ordinary chondrites. In: *Lunar Planet. Sci. XXXVI.* Lunar Planet. Inst., Houston. CD-ROM #1668 (abstract).

Grossman, J.N., Wasson, J.T., 1985. The origin and history of the metal and sulfide components of chondrules. *Geochim. Cosmochim. Acta* **49**, 925–939.

Hewins, R.H., Yu, Y., Zanda, B., Bourot-Denise, M., 1997. Do nebular fractionations, evaporative losses, or both, influence chondrule compositions? *Antarct. Met. Res.* **10**, 275–298.

Johnson, C.M., Beard, B.L., Beukes, N.J., Klein, C., O'Leary, J.M., 2003. Ancient geochemical cycling in the Earth as inferred from Fe isotope studies of banded iron formations from the Transvaal Craton. *Contrib. Miner. Petrol.* **144**, 523–547.

Kehm, K., Hauri, E.H., Alexander, C.M.O'D., Carlson, R.W., 2003. High precision iron isotope measurements of meteoritics material by cold plasma ICP-MS. *Geochim. Cosmochim. Acta* **67**, 2879–2891.

Kong, P., Palme, H., 1999. Compositional and genetic relationship between chondrules, chondrule rims, metal and matrix in the Renazzo chondrite. *Geochim. Cosmochim. Acta* **63**, 3673–3682.

Krot, A.N., Amelin, Y., Cassen, P., Meibom, A., 2005. Young chondrules in CB chondrites: evidence for a giant impact in the early solar system. *Nature* **436**, 989–992.

Larimer, J.W., Wasson, J.T., 1988. Siderophile element fractionation. In: Kerridge, J.F., Matthews, M.S. (Eds.), *Meteorites and the Early Solar System*. University of Arizona Press, Tucson, Arizona, pp. 416–435.

Levasseur, S., Frank, M., Hein, J.R., Halliday, A.N., 2004. The global variation in the iron isotope composition of marine hydrogenetic ferromanganese deposits: implications for seawater chemistry. *Earth Planet. Sci. Lett.* **224**, 91–105.

McSween Jr., H.Y., 1977. On the nature and origin of isolated olivine grains in carbonaceous chondrites. *Geochim. Cosmochim. Acta* **41**, 411–418.

Meibom, A., Petaev, M.I., Krot, A.N., Wood, J.A., Keil, K., 1999. Primitive FeNi metal grains in CH carbonaceous chondrites formed by condensation from a gas of solar composition. *J. Geophys. Res.* **104**, 22053–22059.

Mullane, E., Russell, S.S., Gounelle, M., Mason, T.F.D. 2003a. Iron isotope composition of Allende and Chainpur chondrules: effects of equilibrium and thermal history. In: *Lunar Planet. Sci. XXXIV*. Lunar Planet. Inst., Houston. CD-ROM #1027 (abstract).

Mullane, E., Russell, S.S., Gounelle, M., Mason, T.F.D., 2003b. Iron isotope composition of Allende matrix, CAIs and chondrules. *Meteorit. Planet. Sci.* **39**, A13 (abstract).

Mullane, E., Russell, S.S., Gounelle, M., 2005. Nebular and asteroidal modification of the iron isotope composition of chondritic components. *Earth Planet. Sci. Lett.* **239**, 209–218.

Niles, P.B., Leshin, L.A., Golden, D.C., Socki, R.A., Guan, Y., Ming, D.W., 2005. Modeling Chemical and Isotopic Variations in Lab Formed Hydrothermal Carbonates. In: *Lunar Planet. Sci. XXXVI*. Lunar Planet. Inst., Houston. CD-ROM #2046 (abstract).

Poitrasson, F., Levasseur, S., Teutsch, N., 2005. Significance of iron isotope mineral fractionation in pallasites and iron meteorites for the core–mantle differentiation of terrestrial planets. *Earth Planet. Sci. Lett.* **234**, 151–164.

Radomsky, P.M., Hewins, R.H., 1990. Formation conditions of pyroxene–olivine and magnesian olivine chondrules. *Geochim. Cosmochim. Acta* **54**, 3475–3490.

Reisener, R.J. Goldstein, J.I., 1999. Microstructural and Chemical study of Fe–Ni metal inside Semarkona chondrules. In: *Lunar Planet. Sci. XXX*. Lunar Planet. Inst., Houston. CD-ROM #1868 (abstract).

Richter, F.M., Davis, A.M., Depaolo, D.J., Watson, E.B., 2003. Isotope fractionation by chemical diffusion between molten basalt and rhyolite. *Geochim. Cosmochim. Acta* **67**, 3905–3923.

Roskosz, M., Luais, B., Toplis, M.J. 2005. Experimental determination of iron isotope fractionation during high temperature segregation of metal from silicate liquids: Evaporation or diffusion? In: *Lunar Planet. Sci. XXXVI*. Lunar Planet. Inst., Houston. CD-ROM #1956 (abstract).

Sears, D.W.G., Dodd, R.T., 1988. Overview and classification of meteorites. In: Kerridge, J.F., Matthews, M.S. (Eds.), *Meteorites and the Early Solar System*. University of Arizona Press, Tucson, Arizona, pp. 3–31.

Skulan, F.L., Beard, B.L., Johnson, C.M., 2002. Kinetic and equilibrium Fe isotope fractionation between aqueous FeIII and hematite. *Geochim. Cosmochim. Acta* **66**, 2995–3015.

Taylor, G.J., Scott, E.R.D., Keil, K., 1983. Cosmic setting for chondrule formation. In: King, E.A. (Ed.), *Chondrule and their Origins*. Lunar Planet. Inst., Houston, Texas, pp. 262–278.

Weisberg, M.K., Prinz, M., 1999. Zoned metal in the CR clan chondrites. *AnStarctic Meteorites* **XXIV**, 187–189 (abstract).

Yu, Y., Hewins, R.H., Alexander, C.M.O.'D., Wang, J., 2003. Experimental study of evaporation and isotopic mass fractionation of potassium in silicate melts. *Geochim. Cosmochim. Acta* **67**, 773–786.

Zanda, B., Bourot-Denise, M., Perron, C., Hewins, R.H., 1994. Origin and metamorphic redistribution of silicon, chromium, and phosphorus in the metal of chondrites. *Science* **265**, 1846–1849.

Zanda, B., Bourot-Denise, M., Hewins, R.H., Cohen, B.A., Delaney, J.S., Humayun, M., Campbell, A.J., 2002. Accretion textures, iron evaporation and re-condensation in Renazzo chondrules. In: *Lunar Planet. Sci. XXXIII*. Lunar Planet. Inst., Houston. CD-ROM #1852 (abstract).

Zhu, X.K., Guo, Y., Williams, R.J.P., O'Nions, R.K., Matthews, A., Belshaw, N.S., Canters, G.W., deWaal, E.C., Weser, U., Burgess, B.K., Salvato, B., 2002. Mass fractionation processes of transition metal isotopes. *Earth Planet. Sci. Lett.* **200**, 47–62.